Strain-induced confinement in $Si_{0.75}Ge_{0.25}$ ($Si/Si_{0.5}Ge_{0.5}$) (001) superlattice systems

Ian Morrison, M. Jaros, and K. B. Wong
Department of Theoretical Physics, The University of Newcastle-upon-Tyne, Newcastle-upon-Tyne NE1 7RU, Tyne and Wear, United Kingdom

(Received 15 October 1985; revised manuscript received 1 December 1986)

We report pseudopotential calculations of the electronic structure of strained-layer superlattices consisting of Si and $Si_{0.5}Ge_{0.5}$, with periods in the range 20—140 Å. In our calculation, both the effect of the microscopic crystal potential and that of the strain peculiar to the choice of $Si_{0.75}Ge_{0.25}$ as a buffer layer are taken into account. The superlattice energy levels and wave functions are obtained in the wave-vector space by expanding the wave function in terms of the eigenfunctions of a bulk crystal Hamiltonian of the buffer layer. In this representation, the superlattice wave function is uniquely determined by a set of bulk wave vectors and the optical matrix elements can be obtained directly from the corresponding expansion coefficients. We assume the strain is uniform in both constituents with the lattice constant parallel to the interfaces being determined by the choice of buffer layer. Two different strain configurations are then investigated: firstly the lattice separation in directions perpendicular to the interfaces being the same as in the unstrained bulk constituents and secondly with this lattice separation as in the minimum-energy configuration. A scheme involving the nearly-free-electron model is used to deal with the absolute energies of the constituents. We find that the electron states are confined in the silicon layers, in agreement with existing experimental results. The effective confining barrier in the conduction and valence bands is strain dependent. We model the evolution of the effect of strain upon the formation of confined states and demonstrate that the position of the conduction- and valence-band levels is a sensitive function of strain and well and/or barrier widths. We calculate the optical matrix element across the fundamental superlattice gap and find that the superlattice potential enhances this optical matrix element in ultrathin layers.

I. AN OVERVIEW

It has been demonstrated that structures made of "lattice-mismatched" materials (i.e., with differences between the constituent lattice constants $>0.1\%$) can be grown without a significant number of misfit defects at interfaces provided that the constituent layers are sufficiently thin (~ 100 Å).[1] The lattice mismatch is accommodated by uniform strain. Simple calculations show[2] that the strain field affects the confining barrier height and should be treated on an equal footing with the microscopic potential. This leads to a qualitatively different situation compared to, say, GaAs-$Ga_{1-x}Al_xAs$ structures since the lattice mismatch at the interface may lead to enhanced mixing of Bloch states with different momenta. As a result, weak optical transitions across the fundamental band gap may be significantly enhanced, with interesting opportunities for band-structure engineering. One of the candidates for applications is the Si-Si_xGe_{1-x} superlattice.

Bean *et al.*[3] have achieved high-quality pseudomorphic growth of Si/Si_xGe_{1-x} multilayer structures by molecular beam epitaxy. Much of the interest in this system stems from the possibility of upgrading the existing silicon technology by exploiting the concept of modulation doping to increase mobility. Another interesting opportunity peculiar to this system is offered by the possibility of using Si-based lasers in integrated optics. In both cases successful implementation depends on the understanding of confined states in the superlattice. Some experimental and theoretical results concerning Si/Si_xGe_{1-x} are now available. For example, samples with Si/Si_xGe_{1-x} superlattices grown directly on Si(001) substrates did not show any confinement in the silicon layers. Raman measurements imply that electrons are confined in the alloy layers.[4]

Very recently, Abstreiter *et al.*,[5] reported observations on a $Si/Si_{0.5}Ge_{0.5}$ superlattice grown on $Si_{0.75}Ge_{0.25}$ which were consistent with the existence of electron confinement in the silicon layers. In this structure the substrate is chosen so as to match the lattice constant of the superlattice period. The strain is taken up by both constituent layers (compressive strain in $Si_{0.5}Ge_{0.5}$ and tensile strain in Si). Experiments of Abstreiter *et al.* imply that when strain is included the nature of confinement is quite different in that the states related to the bulk X-point minima of the conduction band in silicon are pushed down relative to their counterparts in the alloy.[5–7] This is illustrated in Fig. 1.

In this study we report calculations based on the pseudopotential method of Jaros *et al.* which has been successfully implemented in unstrained structures.[8,9] Some modifications are required in order to include the effect of strain and these will be described in the following section. The input to the calculations is the best fit of the starting silicon and germanium atomic potentials which ensure a good representation of the band structure of bulk Si and Ge in the relevant range of energies (i.e., the energy sur-

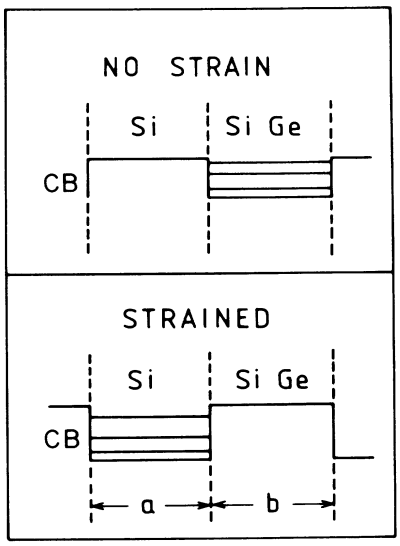

FIG. 1. A sketch of the band offsets of $Si/Si_{0.5}Ge_{0.5}$ superlattices grown on a Si_xGe_{1-x} ($x \sim 0.75$) buffer layer. The way the offsets are expected to change with the inclusion of strain is shown, following the experimental data of Abstreiter *et al.*

faces of the bands near the fundamental gap). A scheme involving the nearly-free-electron model is used to deal with the absolute energies of the constituents.

In the earliest studies of semiconductor superlattices the effect of strain was simply ignored. The first studies in which the effect of strain was taken into account[2] introduced the concept of a free-standing superlattice in which the degree and type of strain was entirely determined by the mutual adjustment of the two constituent materials. This implies that in the direction perpendicular to the interface plane the covalent bonds contract or expand exactly so much as to absorb all elastic energy created by the strain in the plane of the interface. In all strained structures experimentally studied there is evidence of line defects which were formed to relieve the strained interface and pushed by strain fields away from the superlattice into the substrate. It is therefore possible that the lattice constant in the perpendicular direction remains closer to the bulk equilibrium value where it is held by strong bond stretching force constants. Consequently, we have considered both possibilities in this study. It might be argued that in the present context the distinction between the two cases is rather academic. In the structure studied by Abstreiter (which is modeled here) the difference in the perpendicular lattice constants is too small to play a significant part in the zone-folding phenomena we set out to investigate. However, it transpired in the course of our work that the effective conduction-band offset is small and even relatively minor strain-induced shifts of energy levels are worth investigating.

The two different strain configurations which we model in this study are described as follows:

(i) Firstly, the values of $a_\perp$(Si) and $a_\perp$(SiGe), see Fig. 2, are chosen to be the same as in the unstrained bulk constituents. The value of $a_{||}$ is the lattice constant of the overall alloy concentration of the superlattice (i.e., of the buffer layer). This shall be referred to as the bulk $a_\perp$ configuration.

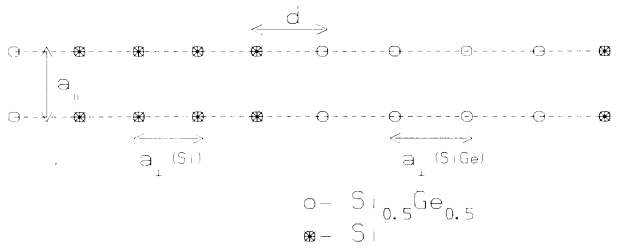

FIG. 2. A schematic drawing showing the atomic positions in the strained superlattices modeled here. The lattice constants associated with the two strain configurations are shown in Table I.

(ii) Secondly, the values of $a_\perp$(Si) and $a_\perp$(SiGe) were calculated by fixing the value of $a_{||}$ to that of the buffer layer and then minimizing the elastic energy of the two constituents.[2] This shall be referred to as the minimum energy configuration.

In all cases the value of d, the lattice spacing across the interface, is the simple average of $a_\perp$(Si) and $a_\perp$(SiGe). The lattice constants associated with these strain configurations are shown in Table I.

For reasons of comparison, a further calculation was performed for each of the superlattices modeled here in which all atomic positions are on a cubic lattice with the lattice constant of the buffer layer. These shall be referred to as the "unstrained" calculations. The atomic positions in the "strained" calculations are shifted from this cubic lattice in the direction perpendicular to the interfaces, the ⟨001⟩ direction. This shifting consists of increasing the atomic spacing between adjacent $Si_{0.5}Ge_{0.5}$ atoms, in the ⟨001⟩ direction, and decreasing the atomic spacing between adjacent silicon atoms. It should be noted that this shifting leaves the size of the superlattice unit cell unchanged.

The results of these calculations are described in Sec. III. In the unstrained cases, we obtain well-confined electron states in the alloy layers. As we pointed out earlier[10] (see also Ref. 11), in both strain configurations considered, the effect of strain is to shift the energies of the confined states at the conduction-band edge and to localize the electron levels in the silicon layers. This confirms the intuitive view of the effect that the strain is expected to have on band gaps of the constituent layers. Both the energy levels and the effective confining power of the super-

TABLE I. The lattice parameters associated with the two strain configurations considered in the text: (I) the bulk $a_\perp$ strain configuration and (II) the minimum-energy strain configuration. The value of $a_{||}$ used in all cases is the lattice constant of the buffer layer and for a buffer layer concentration of $Si_{0.75}Ge_{0.25}$ is 5.4875 Å.

	I	II
$a_\perp$ (Si)	5.43 Å	5.386 Å
$a_\perp$ (Si-Ge)	5.545 Å	5.589 Å

lattice change as a function of the well and barrier width. In the strained calculations the separation between the lowest confined states is larger than the corresponding separation in the unstrained calculations.

The effect of strain is to enhance the mixing in momentum space to accommodate the change of the phase of the total wave function at the interfaces where there is a discontinuity in the lattice separation. This mixing has an enhancing effect on the optical transition probabilities across the fundamental superlattice gap. In the calculation described in Sec. II, the composition of the superlattice wave functions in the wave-vector space is obtained automatically since the solutions are given in terms of the expansion coefficients $A_{n,\mathbf{k}}$. Examination of the expansion coefficients can serve as a basis for a quick assessment of the zone folding. In all the superlattices modeled here, the lowermost conduction-band states are X-like (i.e., these states are derived from the region in $\mathbf{k}$ space near the conduction-band X-point minima of the bulk starting Hamiltonian). The hole state, however, is derived from bulk-valence-band states around $\mathbf{k}=0$ the bulk-valence-band maxima. The magnitude of the optical matrix element across the fundamental superlattice gap reflects the degree of overlap in $\mathbf{k}$ space of the expansion coefficients associated with these states. This optical matrix element is small, due to the small degree of overlap of the two states in $\mathbf{k}$ space. However it is enhanced with the introduction of strain due to the mixing in momentum space of these two states. Rigorous numerical calculations are reported which show that in the structures in question the enhancement of the optical matrix element is quite small except in ultrathin systems. However, it must be stressed that the strength of the effect of strain does reflect the geometrical properties of the structure under investigation and it remains to be seen to what extent the above conclusion is generally valid.

II. METHOD OF CALCULATION

The method of calculation used here is based on the pseudopotential approach of Jaros *et al.*[8,9] Various changes are needed in order to model the strained $Si/Si_{0.5}Ge_{0.5}$ system. The starting point of the calculation is the bulk band structure of a Si_xGe_{1-x} alloy with x corresponding to the overall alloy concentration of the superlattice ($x\sim0.75$ in the superlattices considered here corresponding to Si and $Si_{0.5}Ge_{0.5}$ layers of approximately equal thickness). The superlattice is considered to be grown upon a buffer layer of this overall alloy. The bulk band structure of the buffer layer corresponding to the overall alloy concentration of the superlattice is generated from a Hamiltonian H_0. To this Hamiltonian H_0 is added an additional potential V representing the difference between the potential of the overall ($\sim75\%$) alloy and the actual potential of the superlattice. The form of this potential is as follows:

$$V(\mathbf{r})=\sum_{\mathbf{R}}\left[\sum_{\mathbf{t}_s}V_s(\mathbf{r}-\mathbf{t}_s-\mathbf{R})+\sum_{\mathbf{t}_A}V_A(\mathbf{r}-\mathbf{t}_A-\mathbf{R})-\sum_{\mathbf{t}}V_0(\mathbf{r}-\tau-\mathbf{R})\right], \quad (1)$$

where, V_s, V_A, and V_0 are the atomic pseudopotentials of Si, $Si_{0.5}Ge_{0.5}$, and Si_xGe_{1-x}, respectively, with $x\sim0.75$ corresponding to the overall alloy concentration of the superlattice. $\mathbf{R}$ are the superlattice lattice vectors. $\mathbf{t}_s$, $\mathbf{t}_A$ are the positions of the silicon and the $Si_{0.5}Ge_{0.5}$ atoms, respectively, in the superlattice unit cell. τ are the positions of Si_xGe_{1-x} ($x\sim0.75$) atoms in a cubic structure of the same size and having the same number of atoms as the superlattice. In this model strain is introduced by shifting the positions of the Si and $Si_{0.5}Ge_{0.5}$ atoms in one direction (the $\langle001\rangle$ direction), with respect to the positions of the atoms of the cubic buffer later. The result is a structure which has the lattice constant of Si_xGe_{1-x} ($x\sim0.75$) in the directions parallel to the superlattice interfaces and with the lattice constant of Si in the $\langle001\rangle$ direction, $a_\perp$(Si), being decreased with respect to the buffer and the value of $a_\perp$(SiGe) being increased. As explained earlier two strain configurations have been investigated, (i) the bulk $a_\perp$ configuration and (ii) the minimum-energy configuration. This is the structure experimentally studied by Abstreiter *et al.*[5] The purpose of this approach is to start with the structure of the overall alloy concentration of the superlattice and shifting atoms in the direction of the superlattice axis, so as to achieve a superlattice unit cell of exactly the same size as the corresponding cell in the lattice of the overall alloy.

The atomic pseudopotentials used in (1) are bulk local pseudopotentials which were fitted so as to obtain an accurate account of the band structure of Si and Ge near the band gap. To simplify the numerical procedure, no account of nonlocality and spin-orbit coupling is made in this study. All alloys in the calculation are treated using the virtual crystal approximation for the respective alloy potentials. Although we are aware that these approximations affect the position of the states lying further from the superlattice band edges we do not think that the corresponding corrections can alter significantly the conclusions of this study.

As the results outlined in the following section demonstrate, our model yields the valence-band offsets which are practically the same as those obtained from the local-density total-energy calculations[7] (i.e., they fall within the error that might be incurred as a result of a different choice of the local-density functional). It would appear that the changes in energy levels and band offsets, at least as far as $Si/Si_{0.5}Ge_{0.5}$ systems considered in this study are concerned, are almost entirely due to simple first-order volume-dependent terms in the Hamiltonian, familiar from the nearly-free-electron theory, and can be evaluated without recourse to exacting calculations. Note that the secret of our success lies in the choice of the starting point, i.e., the bulk Hamiltonian of the buffer layer from which we begin is "lattice matched" to the superlattice. The energies of the superlattice states are then calculated from energy differences which are very small compared to the mean-valence-band energy.

To set up our calculation, the superlattice wave functions ψ are expanded in terms of the eigenfunctions of the buffer layer [Si_xGe_{1-x} ($x\sim0.75$)] $\phi_{n,\mathbf{k}}$ (where n represents the band index and $\mathbf{k}$ the wave vector). This gives an equation of the form

$$(\hat{H}_0+\hat{V}-E)\Psi=0\ , \tag{2}$$

with

$$\Psi=\sum_{n,\mathbf{k}} A_{n,\mathbf{k}}\phi_{n,\mathbf{k}}\ ,$$

$$\hat{H}_0\phi_{n,\mathbf{k}}=E_{n,\mathbf{k}}\phi_{n,\mathbf{k}}\ . \tag{3}$$

Since the potential, $\hat{V}$, has the period of the superlattice then, by Bloch's theorem, the values of $\mathbf{k}$ needed in the expansion are equal to $\mathbf{k}_s+\mathbf{g}$, where $\mathbf{k}_s$ is a reduced wave vector in the superlattice Brillouin zone and $\mathbf{g}$ is a superlattice reciprocal lattice vector. Most calculations performed here are done at the center of the superlattice Brillouin zone (Γ), see Fig. 3, corresponding to $\mathbf{k}_s=\mathbf{0}$. This unique definition of Ψ is then used in (2) and the equation multiplied from the left by $\phi^*_{n'\mathbf{k}'}$, then integrating over all space gives us the secular equation of the form

$$A_{n\mathbf{k}}(E_{n\mathbf{k}}-E)\delta_{nn'}\delta_{\mathbf{k}\mathbf{k}'}+\frac{1}{\Omega}\sum A_{n,\mathbf{k}}\int \phi^*_{n'\mathbf{k}'}\hat{V}\phi_{n\mathbf{k}}\,d^3r=0\ , \tag{4}$$

where Ω is the total volume of the crystal. This secular equation is solved numerically by a direct diagonalization procedure to give eigenvalues E, and eigenvectors $A_{n,\mathbf{k}}$.

Since the bulk eigenfunctions $\phi_{n\mathbf{k}}$ of Eq. (3) used as a basis set in the expansion of the superlattice wave functions are described in the form of plane-wave expansions, the matrix element of the potential between two plane waves is needed in setting up the secular equation, i.e.,

$$\frac{1}{\Omega}\langle \mathbf{k}'+\mathbf{G}'\,|\,\hat{V}(\mathbf{r})\,|\,\mathbf{k}+\mathbf{G}\rangle\ , \tag{5}$$

where $\mathbf{G}$ are reciprocal lattice vectors of the bulk buffer layer lattice. $V(\mathbf{r})$ is a local pseudopotential so that (5) can be written as

$$\frac{1}{\Omega}\int e^{-i\mathbf{g}\cdot\mathbf{r}}V(\mathbf{r})\,d^3r\ , \tag{6}$$

with $\mathbf{g}=\mathbf{k}'-\mathbf{k}+\mathbf{G}'-\mathbf{G}$.

Since $\mathbf{k}'-\mathbf{k}$ is a reciprocal lattice vector of the superlattice then $\mathbf{g}$ is also a superlattice reciprocal lattice vector. Hence using the form of the potential in (1), Eq. (6) can be separated into the structure factors and atomic pseudopotentials:

$$\frac{1}{\Omega_{\mathrm{SL}}}\left[V_s(g)\sum_{t_s}e^{i\mathbf{g}\cdot\mathbf{t}_s}+V_A(g)\sum_{t_A}e^{i\mathbf{g}\cdot t_A}+V_0(g)\sum_{\tau}e^{i\mathbf{g}\cdot\mathbf{t}}\right] \tag{7}$$

where

$$V_s(g)=\int e^{i\mathbf{g}\cdot\mathbf{r}}V_s(\mathbf{r})d^3r,\quad V_A(g)=\int e^{i\mathbf{g}\cdot\mathbf{r}}V_A(\mathbf{r})d^3r,\quad V(g)=\int e^{i\mathbf{g}\cdot\mathbf{r}}V_0(\mathbf{r})d^3r\ ,$$

and Ω_{SL} is the volume of the superlattice unit cell. The structure factors in (7) are treated exactly by specifying the exact positions of the constituent atoms in the superlattice unit cell.

The atomic pseudopotentials introduced in (7) are obtained by considering first of all calculations performed on bulk materials using empirical pseudopotentials. The empirical pseudopotentials, evaluated at bulk reciprocal lattice vectors, were chosen so as to ensure an accurate description of the band structures in the relevant energy range (i.e., near the band gap). The absolute energies of the relevant band structures were obtained by using the nearly-free-electron model[12] to evaluate the atomic pseudopotentials at $g=0$ [$V(0)=-\frac{2}{3}E_F$, where E_F is the free-electron Fermi energy], which is calculated using the volume per atom in the relevant crystal. The introduction of $V(0)$ into a calculation on a bulklike crystal simply introduces a rigid shift in the energies of the band structure.

Calculations were then performed on bulk materials (Si and $Si_{0.5}Ge_{0.5}$) varying the volume-dependent kinetic energy terms and $V(0)$ to obtain the volume dependence of the energies of the bulk band edges. The atomic pseudopotentials at nonzero reciprocal lattice vectors were left unchanged. This in effect means varying the kinetic energy terms and the average potential in the bulk Hamiltonians which turn out to be playing a dominant role in determining the band offsets.

The positions of the band edges of silicon and $Si_{0.5}Ge_{0.5}$ with their real lattice constants and the lattice constant of the substrate (Si_xGe_{1-x}, $x\sim0.75$) are displayed in Fig. 4(a). The relative positions of the two band structures (Si and $Si_{0.5}Ge_{0.5}$) with the volume per atom as seen by the strained calculations is then obtained by linearly extrapolating between the two band structures shown in Fig. 4(a) to the appropriate volume per atom. These are the relative alignments of the two band structures where the two constituents have the volume per atom as seen by the strained configurations. These relative alignments for the

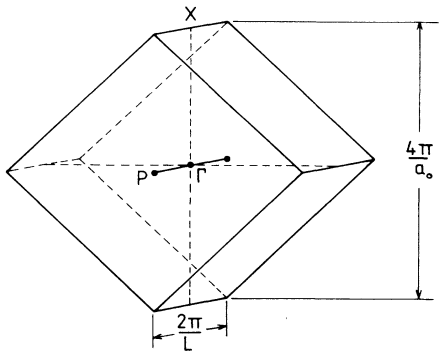

FIG. 3. A sketch of the Brillouin zone of the superlattice, with the special points Γ, P, and X shown.

two strained configurations are shown in Fig. 4(b). In the final superlattice calculation the introduction of uniaxial strain will produce further shifts and splitting in the band edges.

The atomic pseudopotentials to be used in the superlattice calculation are then obtained from the appropriate values at the first three nonzero reciprocal lattice vectors. The potentials at $\mathbf{g}=0$ are adjusted so as to reproduce the band offsets shown in Fig. 4(b) in the unstrained calculations, (the configuration in which all atomic positions are in the cubic lattice of the buffer layer). A functional fit is used to extrapolate between the values at these bulk reciprocal lattice vectors. To facilitate smooth truncation, which occurs at $\mathbf{g}=(4,0,0)$, the potential has a node at the next two reciprocal-lattice vectors [i.e., (2,2,2) and (4,0,0)].

The actual point of truncation is unimportant provided that the potential is truncated in a continuous fashion. Indeed it has been demonstrated[13] that making the potential discontinuous may lead to a significant error. The precise form of the potential between the bulk reciprocal lattice vectors is also unimportant as results derived from various different functional fits lead to virtually identical

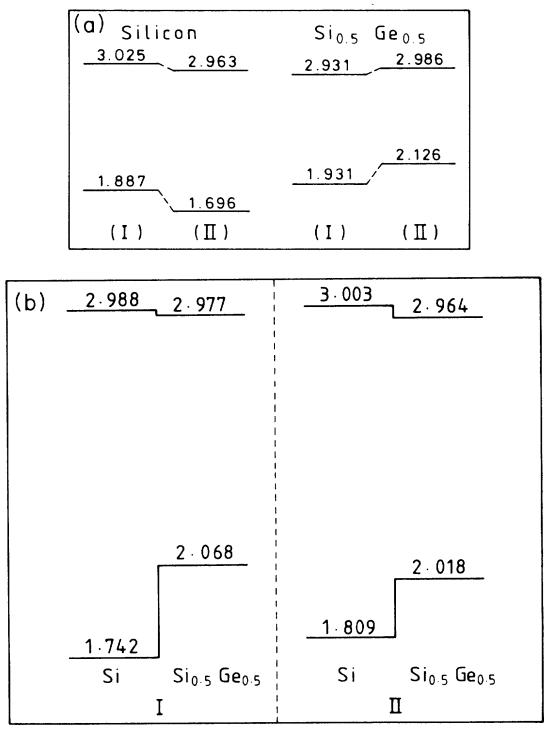

FIG. 4. (a) The positions of the conduction- and valence-band edges in silicon and $Si_{0.5}Ge_{0.5}$ [using the nearly-free-electron model to evaluate $V(0)$], for the materials with (I) their actual volume per atom and (II) with the volume per atom of $Si_{0.75}Ge_{0.25}$ (all energies are in eV). (b) The position of the (average) conduction- and valence-band edges of Si and $Si_{0.5}Ge_{0.5}$ with the volume per atom as seen by the two strain configurations (I) the bulk $a_\perp$ strain configuration and (II) the minimum-energy strain configuration. The band-structure calculations leading to these results are described in the text.

results. The potential representing silicon in the present calculation is shown in Fig. 5. The form of the functional fit used is (for all of the atomic pseudopotentials)

$$V(g)=\begin{cases} a_1+a_2g^2+a_3g^3+a_4g^4, & 0.0<g<3.2 \\ \exp[7(3-g)](b_1+b_2g+b_3g^2+b_4g^3+b_5g^4), & 3.2<g<4.0 \\ 0, & 4.0<g, \end{cases} \tag{8}$$

with potential at $g=3.2$ being matched to the first derivative. The a_i and b_i are constants and their values for the fit of silicon are shown in Table II. The units of g used here are $2\pi/A_0$ where A_0 is the lattice constant of the buffer layer.

In this procedure for fitting the atomic pseudopotentials, as a first approximation, no account was taken of the volume dependence at nonzero bulk reciprocal lattice vectors. This in effect means neglecting the change in magnitude of the potential due to the change in length of the reciprocal lattice vectors and ignoring the corresponding factor which renormalizes the atomic pseudopotentials to volumes as seen in the strained superlattice.

To see that this constitutes a reasonable approximation, consider first of all, $\mathbf{g}$ parallel to the superlattice interfaces. Since the atomic positions of silicon and $Si_{0.5}Ge_{0.5}$ in directions parallel to the interfaces are the same, then for symmetric wells and/or barriers we can write

$$\sum_{t_s} e^{i\mathbf{g}\cdot\mathbf{t}_s} = \sum_{t_A} e^{i\mathbf{g}\cdot\mathbf{t}_A} . \tag{9}$$

Hence the actual superlattice potential used in (7) can be written

$$\sum_{t_s} e^{i\mathbf{g}\cdot\mathbf{t}_s} [V_s(\mathbf{g})+V_a(\mathbf{g})] . \tag{10}$$

Now taking into account the change in magnitude of the bulk reciprocal lattice vectors from the relevant materials

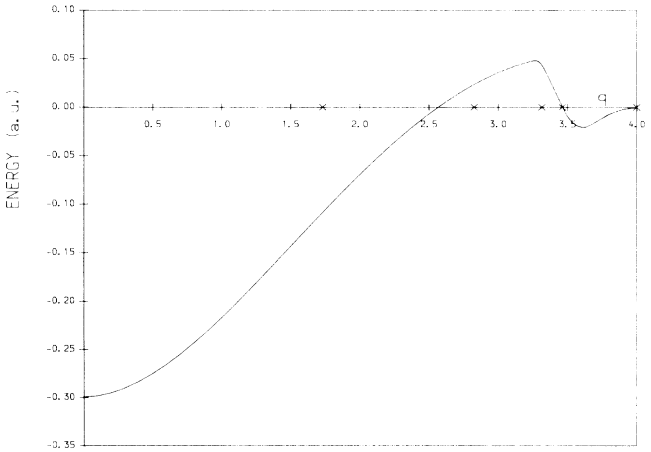

FIG. 5. The atomic pseudopotential for silicon used in the calculation and tabulated in Table II. The position of the bulk reciprocal-lattice vectors is also shown (x). The units of g used are $2\pi/A_0$ where A_0 is the lattice constant of the substrate.

TABLE II. The coefficients used in the expansion of the silicon potential as described in the text. The units of energy are atomic units and the units of the wave vector are $2\pi/A_0$, where A_0 is the lattice constant of the buffer layer.

a_1	−0.298 830 000 0	b_1	2930.960 939 089 7
a_2	0.110 708 905 4	b_2	−3443.048 469 957 7
a_3	−0.031 124 908 5	b_3	1512.458 527 614 3
a_4	0.002 203 672 5	b_4	−294.378 829 952 8
		b_5	21.414 615 687 0

to the materials with the structure as seen by the strained superlattices we can write

$$\mathbf{g}=\mathbf{g}_s-\delta\mathbf{g}$$

and

$$\mathbf{g}=\mathbf{g}_A+\delta\mathbf{g}\ , \tag{11}$$

where $\mathbf{g}_s$ and $\mathbf{g}_A$ are the respective values if no account of the change in lattice constant is taken. Expanding $V_s(\mathbf{g})$ and $V_A(\mathbf{g})$ to first order gives

$$\begin{aligned} V_s(\mathbf{g})&=V_s(\mathbf{g}_s)-\delta g\ V_s'(\mathbf{g}_s)\ , \\ V_A(g)&=V_A(\mathbf{g}_A)+\delta g\ V_A'(\mathbf{g}_A)\ , \end{aligned} \tag{12}$$

since the potentials of silicon and $Si_{0.5}Ge_{0.5}$ are very similar, in summing the expansions in (12) a large degree of cancellation is expected between the first-order terms.

This argument does not apply if $\mathbf{g}$ is perpendicular to the superlattice interfaces since the atomic positions of the two constituents in this direction are very different. However, it is worth stressing that the net volume dependence of the short-wavelength components of the microscopic potential is weak. Consider scattering events perpendicular to the superlattice interfaces. The potential at $\mathbf{g}=(1,1,1)$ will dominate these scattering events (simply compare its magnitude to the potential at other nonzero bulk reciprocal lattice vectors). Taking into account the volume dependence of the reciprocal lattice vector (1,1,1) as one goes from bulk silicon to the silicon as seen by the strained calculation means reducing its magnitude. This also means that the potential associated with (1,1,1) should be increased slightly. However, taking into account the renormalization of the atomic pseudopotential to the volume as seen in the strained calculation implies multiplying the potential by a factor Ω_s/Ω_s', where Ω_s is the volume per atom of bulk silicon and Ω_s' is the corresponding volume seen by the strained calculation. This factor is less than unity and at (1,1,1) tends to cancel the volume correction due to the change in magnitude of the reciprocal lattice vectors. A similar argument applies when considering scattering events in the alloy. This is well in keeping with our earlier observations indicating the dominant role of the kinetic energy and the long-wavelength potential-energy terms in determining the band lineup.

A check on the accuracy of our numerical procedure based on (4) can be performed by filling the superlattice unit cell with Si and $Si_{0.5}Ge_{0.5}$, respectively, with the atoms in the unstrained cubic lattice. This should reproduce the bulk band structure of silicon and $Si_{0.5}Ge_{0.5}$ executed with the lattice constant of the $Si_{0.75}Ge_{0.25}$ and with the $V(0)$'s corrected accordingly. This is indeed achieved with a meV accuracy. Doing this tells us the value of the band offsets as seen by the unstrained calculations. This procedure cannot be repeated in the case of the strained calculations as filling the superlattice with one of the constituents using the strained lattice parameters would result in a unit cell of different size. Hence no direct determination of the strained band offsets is possible. It is only possible, by examining the confinement of the superlattice states, to estimate where the band edges lie.

III. NUMERICAL RESULTS

As explained previously, for reasons of comparison, an unstrained and strained calculation were performed on each structure studied. In the unstrained structures all atomic positions are the same as in the bulk (cubic) buffer layer. In the strained calculations the atomic positions were shifted in directions perpendicular to the interfaces changing the lattice constants of the constituents in this direction, i.e., introducing uniaxial strain. As explained previously two configurations of strain were investigated, namely, (i) the bulk $a_\perp$ configuration, and (ii) the minimum energy configuration. The results concerning these two strain configurations are described in Secs. III A and III B, respectively.

A. Results for the bulk $a_\perp$ configuration of strain

Firstly, let us deal with the results concerning the bulk $a_\perp$ configuration of strain. Three different periods of superlattice were investigated (20, 70, and 140 Å). The actual sizes of these three systems are as follows:

(i) The 20-Å-period case consists of a superlattice with eight silicon atoms and eight $Si_{0.5}Ge_{0.5}$ atoms in the unit cell. This results in a superlattice of period 21.95 Å and an overall alloy concentration of $Si_{0.75}Ge_{0.25}$.

(ii) The 70-Å-period case consists of a superlattice with 28 silicon atoms and 24 $Si_{0.5}Ge_{0.5}$ atoms in the unit cell. This results in a superlattice of period 71.28 Å and an overall alloy concentration of $Si_{0.77}Ge_{0.23}$.

(iii) The 140-Å-period case consists of a superlattice with 52 silicon atoms and 48 $Si_{0.5}Ge_{0.5}$ atoms in the unit cell. This results in a superlattice of period 137.1 Å and an overall alloy concentration of $Si_{0.76}Ge_{0.24}$.

In the latter two cases the asymmetry in the well widths was chosen to rule out any high-symmetry effects which may result from the more symmetric cases corresponding to equal numbers of silicon and $Si_{0.5}Ge_{0.5}$ atoms in the superlattice unit cell.

The positions of the lowest conduction-band energies in all calculations with this strain configuration are displayed in Fig. 6. All energies are measured from the top of the valence band of $Si_{0.5}Ge_{0.5}$ (with lattice constant corresponding to $Si_{0.75}Ge_{0.25}$). All conduction states described here are doubly degenerate in character, the degeneracy arising from the flat structure of the bulk X minima, see Sec. III D. Also shown on this diagram are the positions of the conduction-band minima (the minima

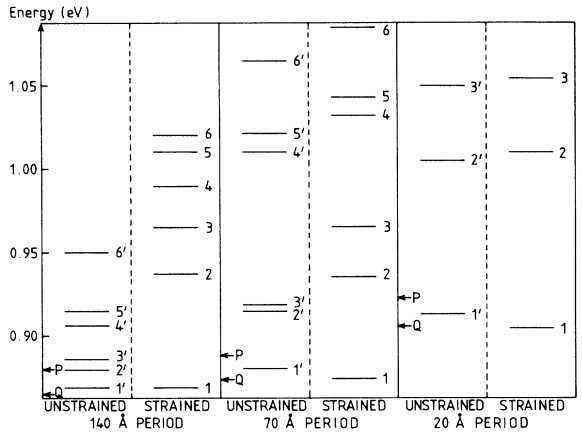

FIG. 6. The energy levels of the superlattice conduction-band states, at the center of the Brillouin zone, in the bulk $a_\perp$ strain configuration. Results of both the "strained" and "unstrained" calculations are shown for superlattice periods of 140, 70, and 20 Å. All energies being doubly degenerate. All energies are measured from the valence-band edge of unstrained $Si_{0.5}Ge_{0.5}$. Also shown are the conduction-band edges of Si, P, and $Si_{0.5}Ge_{0.5}$, Q, as seen by the unstrained calculation in each case. Note how these values move up in energy as the well width is reduced. This is because as the period is reduced the number of sampling points between Γ and X is reduced, hence states at the actual minimum of the conduction band of Si and $Si_{0.5}Ge_{0.5}$ are not reproduced by the superlattice calculations.

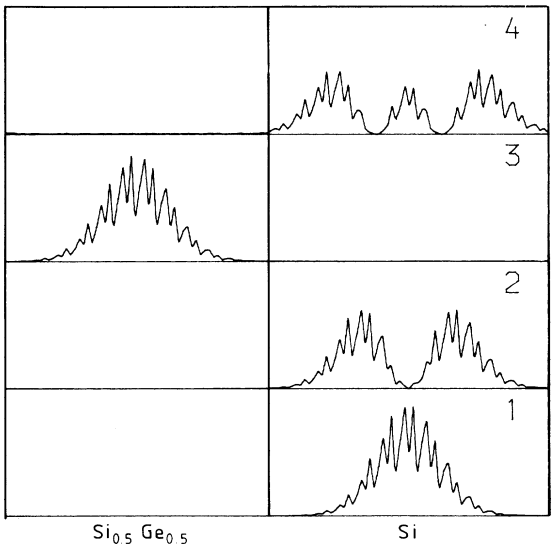

FIG. 7. Charge densities, summed over degeneracies, generated at the center of the superlattice Brillouin zone (Γ) of the first four conduction-band states in the 140-Å-period strained superlattice calculation, in the bulk $a_\perp$ strain configuration. We plot these charge densities along a line in the $\langle 001 \rangle$ direction going through bond centers. Arbitrary units are used with all states being normalized to the maximum charge density of the first state, as is the case in all the charge densities presented here.

near the X point of the bulk Brillouin zone) of silicon (P) and $Si_{0.5}Ge_{0.5}$ (Q), as seen by the unstrained calculation. These are the so-called conduction-band offsets and are calculated by filling the unstrained superlattice with silicon and $Si_{0.5}Ge_{0.5}$, respectively, as described in Sec. II. It is not possible to calculate these offsets in the strained calculation in such a manner as filling the superlattice with either silicon or $Si_{0.5}Ge_{0.5}$ would result in a superlattice cell of different size. However, estimations of the strained band offsets have been made and will be described later.

The effective conduction-band edges, i.e., as "seen" by the superlattice calculation performed at point Γ of the superlattice Brillouin zone, increase in energy as the well width is reduced. This is due to the decrease in the number of sampling points needed in the bulk Brillouin zone to describe ψ of (3) as the superlattice period is reduced. In the case of the 20-Å-period calculation nine $\mathbf{k}$ points must be included from the line $-X$ to X. Hence the calculation does not "see" the actual conduction-band minimum of silicon or $Si_{0.5}Ge_{0.5}$, the nearest sampling point being away from the minima and hence of higher energy. If calculations were performed with $\mathbf{k}_s$ ($\mathbf{k}_s$ being the reduced wave vector in the superlattice Brillouin zone), away from Γ on the line Γ to P in the superlattice Brillouin zone, see Fig. 3, then for a certain value of $\mathbf{k}_s$ the calculation would see the actual conduction-band minima of silicon and $Si_{0.5}Ge_{0.5}$ and a band offset in the conventional sense (familiar from simple semiclassical methods) would be recovered.

Figure 7 shows the charge densities of the first four conduction-band states in the 140-Å-period strained calculation. The charge densities are summed over the doubly degenerate states, as are all conduction state charge densities presented here. These are charge densities along a line in the $\langle 001 \rangle$ direction going through bond centers. The first two states are confined in the silicon layers in agreement with the sketch of band offsets presented in Fig. 1. These states exhibit a very high degree of confinement and are practically dispersionless. The separation between states 1 and 2 localized in silicon is markedly increased in going from the unstrained to the strained calculation. Since state 3 is localized in the alloy the effective confining barrier in this structure lies between levels 2 and 3.

Figure 8 shows plots of the values of $|A_{n\mathbf{k}}|^2$, summed over the degeneracy, for the states shown in Fig. 7, along the line $-X$ to X in the bulk Brillouin zone of the $Si_{0.76}Ge_{0.24}$ alloy. Coefficients from five bands are shown in ascending band order in the figure, (i.e., the highest three valence bands and lowest two conduction bands). The plots show that all confined states are derived from around the X minima of the lowest conduction band. Figures 9 and 10 show the corresponding states for the 70-Å-period calculation. These states are slightly less well confined than in the 140-Å-period case. Figures 11 and 12 show the corresponding states for the 20-Å-period calculation. The degree of confinement is again less than in the two preceding cases.

Figures 13 and 14 show the first four conduction-band-state charge densities, summed over the double de-

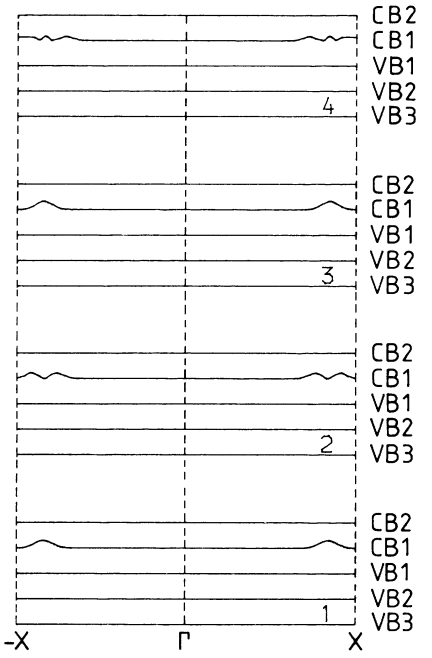

FIG. 8. Plots of the wave-function coefficients, $|A_{n\mathbf{k}}|^2$, (summed over degeneracies) associated with the states shown in Fig. 7, as a function of the wave vector ($\mathbf{k}$) in the bulk Brillouin zone of $Si_{0.76}Ge_{0.24}$. The $\mathbf{k}$ vector runs from $-X$ to X through Γ. Coefficients belonging to five bands (n) are shown; VB1, VB2, and VB3 are the uppermost valence bands and CB1, CB2 the lowermost conduction bands. The vertical scaling is such that the spacing between bands is unity.

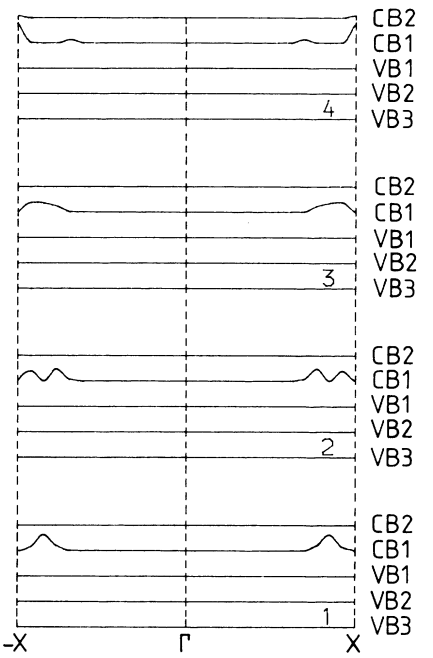

FIG. 10. Plots of the $|A_{n\mathbf{k}}|^2$ associated with the states shown in Fig. 9.

generacy, in the 70-Å-period unstrained calculation. In this case the lowest state is confined in the $Si_{0.5}Ge_{0.5}$ layer and not in the silicon layer as in the corresponding strained calculation (Fig. 9). Also the degree of confinement in all the states is much less than in states of the corresponding strained calculation. This is in agreement with the sketch of band offsets presented in Fig. 1. In all

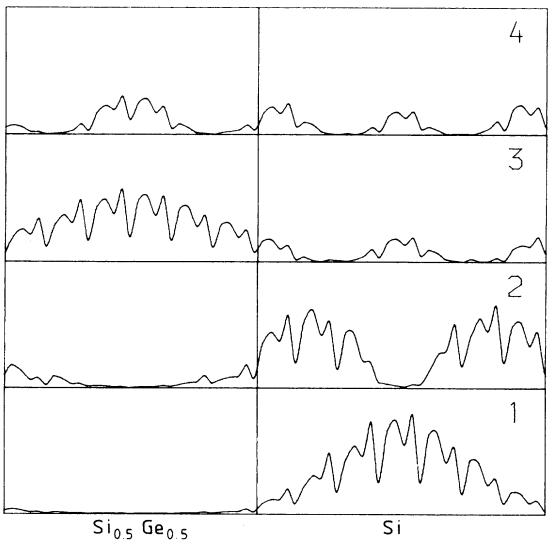

FIG. 9. Charge densities of the first four conduction-band states in the 70-Å-period strained calculation, in the bulk $a_\perp$ strain configuration.

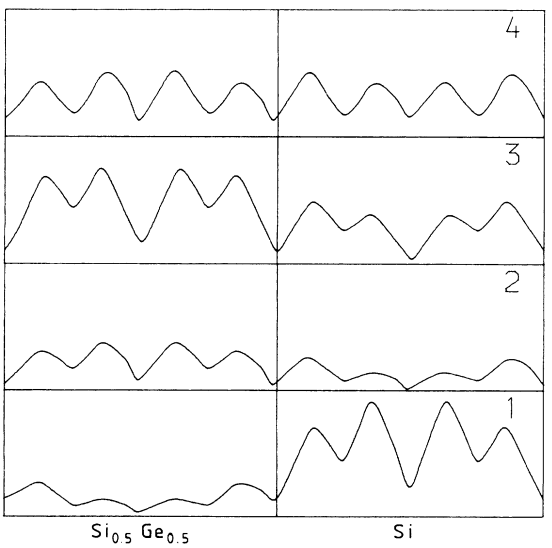

FIG. 11. Charge densities of the first four conduction band states in the 20-Å period strained calculation, in the bulk $a_\perp$ strain configuration.

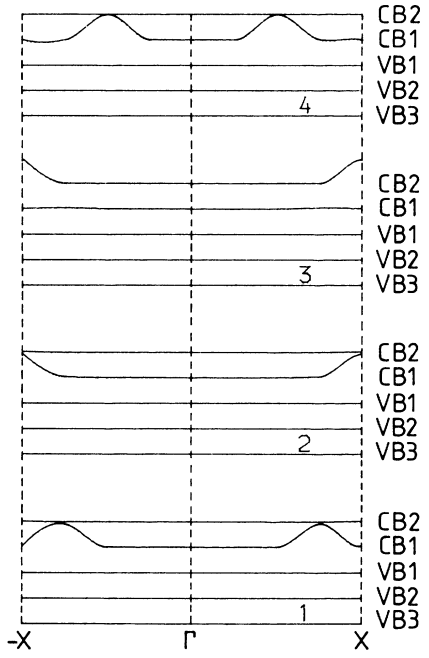

FIG. 12. Plots of the $|A_{nk}|^2$ associated with the states shown in Fig. 11.

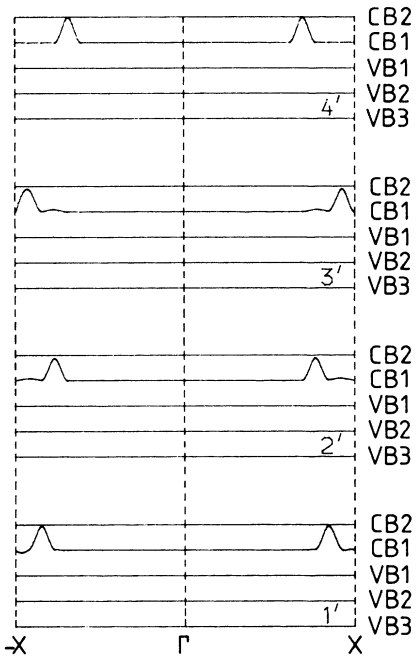

FIG. 14. Plots of the $|A_{nk}|^2$ associated with the states shown in Fig. 13.

these cases the higher-lying states exhibit a similar behavior to those seen in $GaAs/Ga_xAl_{1-x}As$ systems.

Figures 15 and 16 show the top four valence band states in the 70-Å-period strained calculation, and in Fig. 17 are shown the energies of these states together with the energies of the corresponding states in the unstrained calculation. All these states are confined in the $Si_{0.5}Ge_{0.5}$ region as the well depth due to the valence-band offsets is very large ($\sim$300 meV). The energies are again measured from the valence-band edge of $Si_{0.5}Ge_{0.5}$ as seen by the unstrained calculation. The strain-induced splitting of the top of the valence band ($\sim$30 meV) is in good agreement with calculations performed by People[6] after taking into account the fact that his calculations were performed for superlattices grown on silicon and not on Si_xGe_{1-x} ($x \sim 0.75$) as is performed here. It is worth commenting

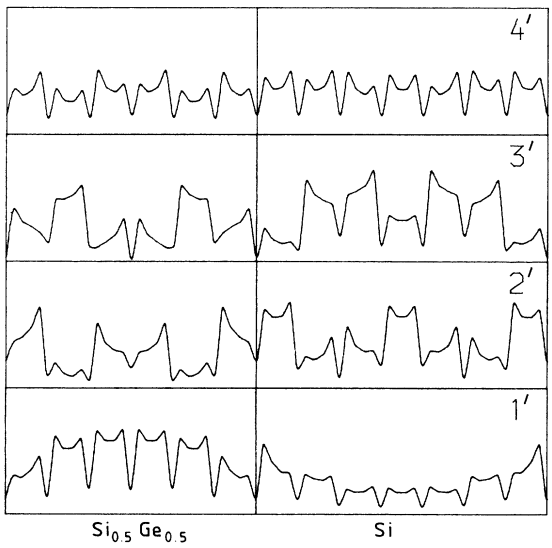

FIG. 13. Charge densities of the first four conduction-band states in the 70-Å-period unstrained calculation.

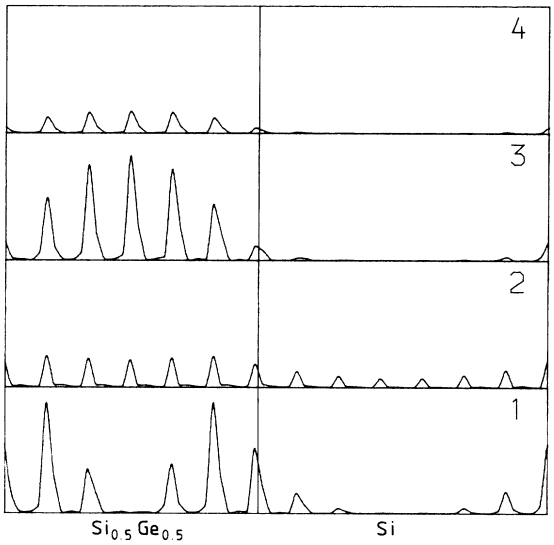

FIG. 15. Charge densities of the highest four states derived from the valence band in the 70-Å-period strained calculation, in the bulk $a_\perp$ strain configuration.

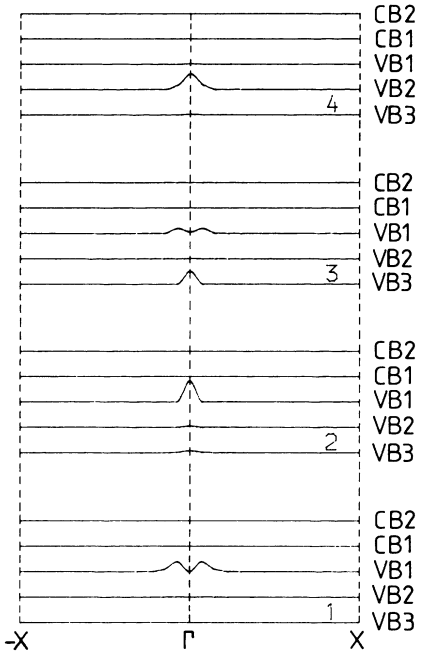

FIG. 16. Plots of the $|A_{nk}|^2$ associated with the states shown in Fig. 15.

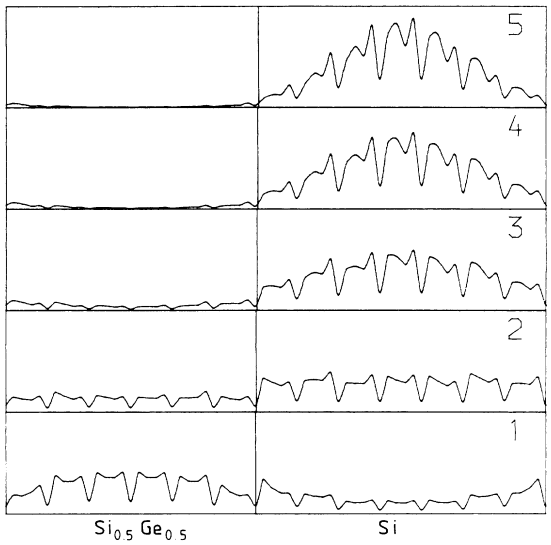

FIG. 18. Charge densities for the first conduction-band state with the slow inclusion of strain, in the 70-Å-period calculation with the bulk $a_\perp$ strain configuration. The effect on the confinement of the state as strain is increased is clearly seen as you go from state 1 (unstrained) to state 5 (fully strained, as in the bulk $a_\perp$ strain configuration).

that magnitudes of the charge densities seen here are peculiar to the direction along one line in the ⟨001⟩ direction (through the bond). If a different line were chosen some changes in the magnitudes of these charge densities would be seen. It is the sum of such plots which should be used to make a quantitative comparison with the conventional envelope functions.

In the 70-Å-period calculation the effect of evolution of

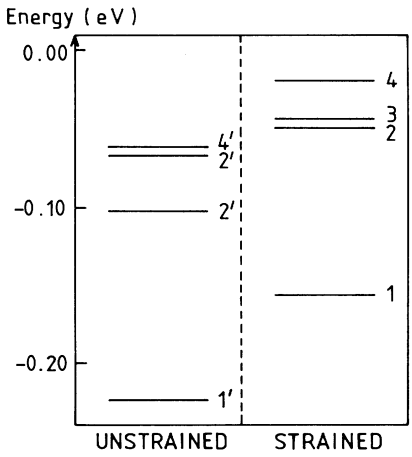

FIG. 17. Energy eigenvalues from states derived from the top of the valence band in the 70-Å-period calculation, in the bulk $a_\perp$ strain configuration. Results for both the strained and unstrained calculations are shown, all energies being measured from the valence-band edge of $Si_{0.5}Ge_{0.5}$ as seen in the unstrained calculation.

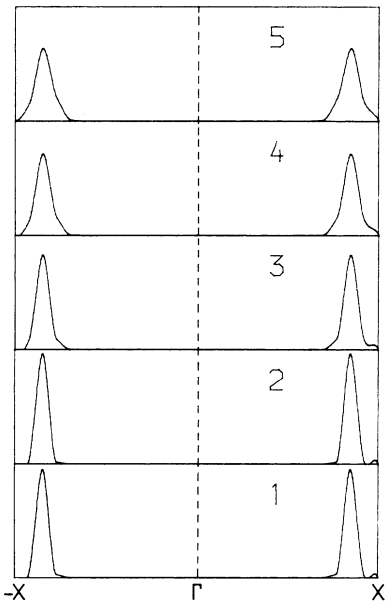

FIG. 19. The variation of the $|A_{n,\mathbf{k}}|^2$ with the slow inclusion of strain, corresponding to the charge densities shown in Fig. 18. Only contributions from the first conduction band (CB1) are shown (all other bands having little or zero contribution). The **k** vector runs from $-X$ to X through Γ in the bulk Brillouin zone of $Si_{0.77}Ge_{0.23}$. It is clearly shown how the $|A_{n,\mathbf{k}}|^2$ spread out in **k** space as strain is increased. The vertical scaling is such that the spacing between plots is unity.

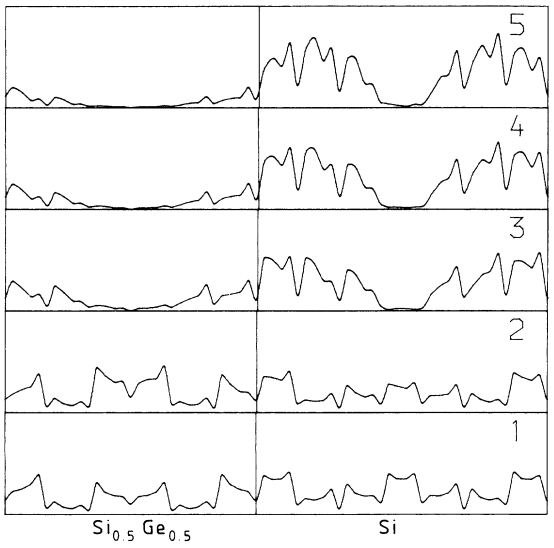

FIG. 20. Charge densities for the second conduction-band state with the slow inclusion of strain, in the 70-Å-period calculation with the bulk $a_\perp$ strain configuration. It is clearly shown how the state changes from one with no particular confinement in the unstrained case, state 1, to the first excited state confined in silicon in the fully strained case, state 5, strained as in the bulk $a_\perp$ strain configuration.

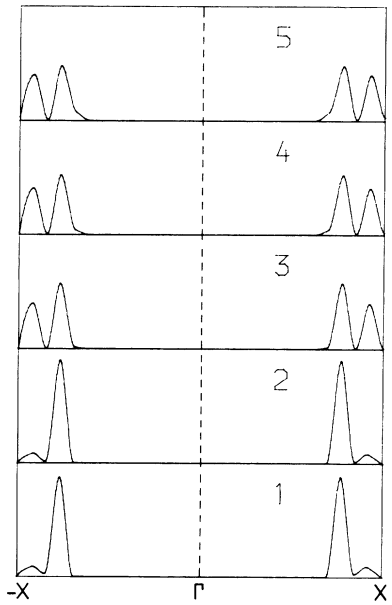

FIG. 21. The variation of the $|A_{nk}|^2$ with the slow inclusion of strain corresponding to the charge densities shown in Fig. 20, only contributions from the first conduction band are shown. It is clearly shown how the state changes from having a single peak around the X minimum to having a double peak around the X minimum corresponding to the first excited state confined in silicon.

strain induced states were investigated. The atomic positions in the ⟨001⟩ direction were changed in steps from the unstrained case, where all atomic spacings are equal to those in $Si_{0.77}Ge_{0.23}$, to the strained case where the atomic spacing in the ⟨001⟩ direction is equal to the atomic spacing in silicon and $Si_{0.5}Ge_{0.5}$, respectively. The effect on the first conduction-band-state charge densities is shown in Fig. 18. The state changes from being confined in $Si_{0.5}Ge_{0.5}$ to being confined in the silicon. As the atomic positions are shifted more and more the degree of confinement increases. Figure 19 shows the values of $|A_{nk}|^2$ for the states shown in Fig. 18. Only contributions from the first conduction band used in the expansion are shown, contributions from other bands being negligible. Note that the amount of the Brillouin zone needed to describe the confined state increases as the strain is increased. This explains the increase in the separation of the adjacent confined levels obtained in the strained calculation. Figures 20 and 21 show the corresponding results for the second conduction-band state. In this case the charge densities change from showing no particular confinement with no strain to the first excited state confined in silicon. Corresponding changes are seen in the values of $|A_{nk}|^2$.

B. Results for the minimum-energy configuration of strain

Secondly, consider calculations performed with the atomic positions in the minimum-energy configuration. Two superlattice periods were chosen here, 20 and 44 Å. The actual sizes of these two systems are as follows:

(i) The 20-Å-period case consists of a superlattice with eight silicon atoms and eight $Si_{0.5}Ge_{0.5}$ atoms in the unit cell. This results in a superlattice of period 21.95 Å and an overall alloy concentration of $Si_{0.75}Ge_{0.25}$. This system is the same as the preceding 20-Å case except for the values of $a_\perp$(Si) and $a_\perp$(SiGe).

(ii) The 44-Å-period case consists of a superlattice with 16 silicon atoms and 16 $Si_{0.5}Ge_{0.5}$ atoms in the unit cell. This results in a superlattice of period 43.90 Å and an overall alloy concentration of $Si_{0.75}Ge_{0.25}$.

The energies in the strained configurations of these two structures are displayed in Fig. 22. As in the previous strain configuration the effect of shifting the atoms in the ⟨001⟩ direction results in the confinement of the first conduction-band state changing from the alloy to the silicon layers. The wave functions associated with these states show a great deal of similarity to the bulk $a_\perp$ strain configuration and are not shown here. Comparison of the eigenvalues of the two 20-Å-period strained calculations shows a 20-meV increase in the separation of the valence- and conduction-band states in going from the bulk $a_\perp$ strain configuration to the minimum-energy strain configuration. There is also an increase in the separation of the first two conduction-band states of about 20 meV.

C. Discussion of the accuracy of the calculation

In our calculational procedure we limit the number of bands used in our expansion of the superlattice wave functions. In the calculations presented here seven bands have been used in the expansion set, the three uppermost valence bands and the first four conduction bands. As

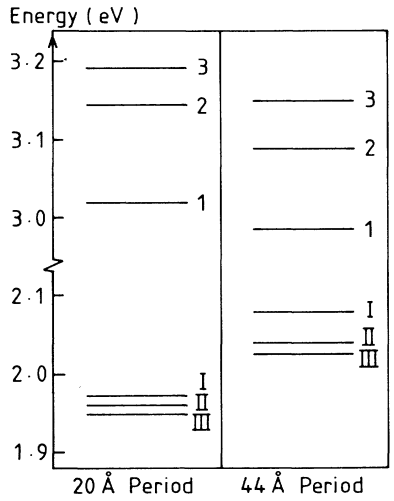

FIG. 22. Energy eigenvalues associated with the 20- and 44-Å-period strained calculations with the atomic positions in the minimum-energy configuration. All energies are measured from the valence-band edge of $Si_{0.5}Ge_{0.5}$ as seen by the unstrained calculation.

has been demonstrated in $Ga_{1-x}Al_xAs$ systems[8,9] this truncation is well justified since there is very little mixing between the bands. However in the case of strained systems the number of bands included in the expansion set needs to be increased if calculations are to be performed on large-period superlattices. This can be seen by examining Fig. 23; here we have the superlattice band gap plotted against the period. These are the results of seven band calculations for the bulk $a_\perp$ strain configuration. The band gap should approach a constant value as the effects

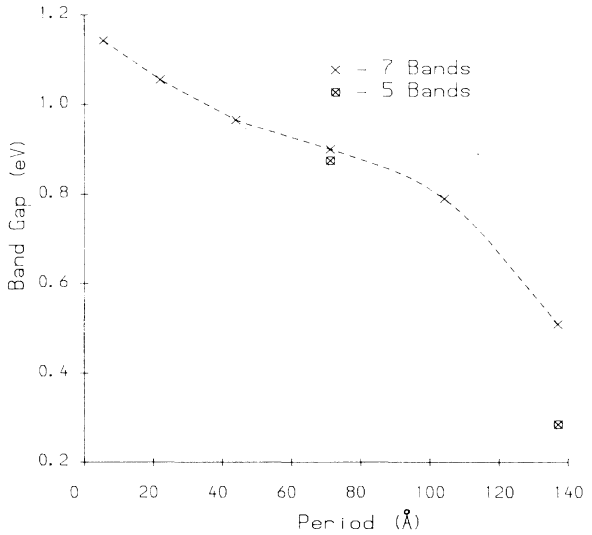

FIG. 23. A plot of the superlattice band gap against the superlattice period for the bulk $a_\perp$ strain configuration. Results of five- and seven-band calculations are shown. From this figure it can be seen how a larger expansion set is needed in order to model large-period superlattices.

of quantum confinement and dispersion become unimportant as the period is increased. This occurs up to a certain limit (period 70 Å corresponding to 52 atoms in the unit cell) after which it falls off, indicating that the number of bands in the expansion set is not large enough.

To demonstrate the breakdown of the calculation for seven bands two results for a five-band calculation are also shown. For 70-Å period the gap is nearly the same whereas for 140-Å period (100 atoms in the unit cell), there is a significant difference. This need for a larger expansion set for large periods is due to the large cumulative shifts of atoms from the positions of the bulk (cubic) buffer layer. With the origin chosen at the center of the alloy layer, the largest atomic shift is for the atoms on either side of the interface. In the 140-Å-period calculation this shift is $\sim 25\%$ of the atomic spacing in this direction (for the bulk $a_\perp$ strain configuration). The expansion set using seven bands is not large enough to cope with this large shift. As can be seen from the figure the largest period which can be modeled accurately with this basis set is about 70 Å corresponding to a maximum shift of atoms of $\sim 12\%$ of the atomic spacing. With the atomic positions in the minimum energy configuration these shifts are even larger hence the maximum period considered in the seven-band model is ~ 44 Å.

D. Estimation of the band alignments and discussion of dispersion

As explained previously there is no direct way of determining the "band offsets" in our strained calculations. However an estimate of where the bulk band edges lie, and therefore the apparent value of the band offsets, can be obtained by examining the confinement of the superlattice states. We have made such an estimate in the case of the 44-Å-period calculation in the minimum-energy strain configuration.

(i) Firstly, consider the valence-band discontinuity. In both constituents the valence-band maxima occur at the center (Γ) of the bulk Brillouin zone, hence one need only consider the superlattice states at Γ in order to assess the valence-band alignment. The barrier must lie somewhere between the two states where the confinement shifts from $Si_{0.5}Ge_{0.5}$ to silicon. We find the valence-band discontinuity must lie somewhere between 312 and 394 meV, (no account of the energy shift due to confinement is considered here). The local-density calculation of Van de Walle and Martin[7,14] was performed on a different system and a direct comparison with their result is not possible. However a linear interpolation to our case yields an offset of 304 meV, in good agreement with our result.

(ii) Secondly, consider the alignments of the conduction-band edges of the two constituents. In order to make a full assessment it is necessary to consider the dispersion throughout the superlattice Brillouin zone and the strain induced splittings of the bulk conduction-band edges. Without strain both constituents have six equivalent minima near to the bulk X points. With the introduction of uniaxial strain (along the z direction) these are split into a twofold degenerate set [the (0,1,0) and (0,0,−1), minima] and a fourfold degenerate set [the

(0,1,0) and (0,−1,0), (1,0,0), and (−1,0,0) minima]. Using the deformation potentials of Ref. 14 and the minimum-energy strain parameters the splitting of these minima have been estimated. In silicon the splitting is ~170 meV with the twofold degenerate valleys being lowest in energy, in $Si_{0.5}Ge_{0.5}$ the splitting is ~171 meV with the fourfold degenerate valleys being lowest in energy.

The dispersion, both perpendicular (z direction) and parallel (y direction) to the interfaces, for the lowest conduction states in the 44-Å-period minimum-energy calculation, has been calculated and are shown in Figs. 24 and 25. The qualitative features of these dispersion curves can be described by considering the zone folding of the bulk band structures under consideration. Looking first of all at the dispersion in the z direction we see two quasidegenerate practically dispersionless bands, the confinement here being in the silicon layer. These originate from the folding in of the bulk silicon minima in the z direction to inside the superlattice Brillouin zone. The quasidegenerate nature originates from the "camel's back" structure of the bulk minima. The dispersionless nature originates from the flat structure of these minima in the z direction; more dispersion is expected in shorter periods.

Now consider the dispersion in the y direction, Fig. 25, parallel to the interfaces. Here two minima are seen. As explained above, the Γ-point minimum originates from the folding in of the bulk silicon minima from the z direction. The minimum near the superlattice X point originates from the bulk minimum in the y direction near the bulk X point (the bulk X point in the y direction maps directly onto the superlattice X point). The effective masses at both of these minima have been calculated, using $\mathbf{k}\cdot\mathbf{p}$ theory, and are shown in the figure. The effective mass at the Γ minimum ($m^*=0.194m_e$ where m_e is the free-electron mass) is very close to the transverse silicon

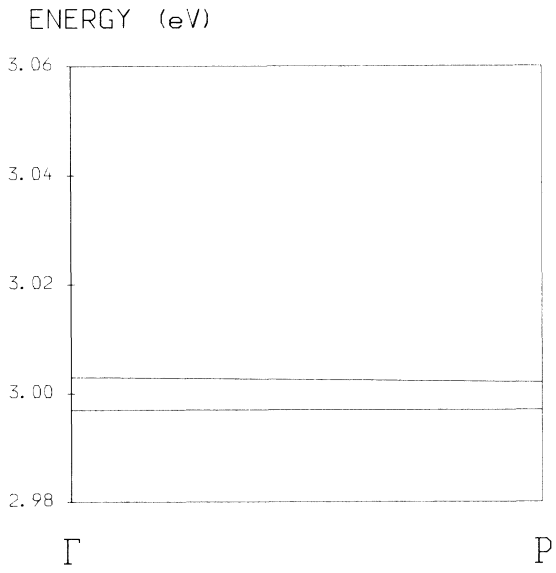

FIG. 24. The dispersion of the lowest conduction states along the line Γ—P (in the Z direction, see Fig. 3) in the 44-Å-period strained calculation in the minimum-energy configuration.

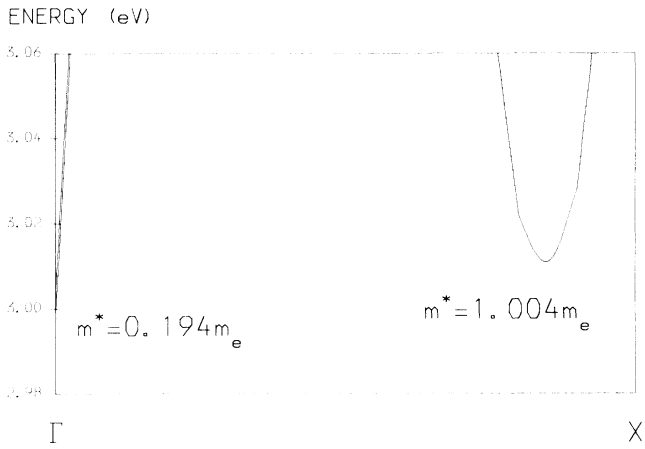

FIG. 25. The dispersion of the lowest conduction states along the line Γ—X (in the y direction, see Fig. 3) in the 44-Å-period strained calculation in the minimum-energy configuration. The effective masses at the minima are shown on the figure, m_e is the free-electron mass.

conduction-band effective mass ($m_\tau=0.19m_e$), as would be expected from the zone-folding picture. The effective mass at the minima near the superlattice X point ($m^*=1.004m_e$) is close to the longitudinal silicon conduction-band effective mass ($m_L=0.98m_e$).

Due to the strain the band discontinuities seen by the calculation at these two minima are very different. At the Γ minima the discontinuity is between the twofold degenerate bulk minima folded in from the z direction. At the minima near the superlattice X point the discontinuity is between the fourfold degenerate bulk minima. At the minimum near the superlattice X point no confinement of charge is seen indicating that the fourfold degenerate bulk minima of the strained constituents are aligned to within a few meV. At the Γ minimum, because of the low effective mass here, it is necessary to estimate the energy shift due to confinement in order to fully assess the band discontinuity seen here. The change in confinement, from silicon to $Si_{0.5}Ge_{0.5}$, occurs between 126 and 195 meV above the lowest confined level in silicon. In order to estimate this shift, Kronig-Penney effective mass type calculations were performed with the effective mass as calculated at Γ and the well or barrier widths of the 44-Å strained minimum-energy calculation, varying the height of the barrier. The picture of confinement is best described with a barrier height in the range 250 to 300 meV, with the shift in energy of the first confined state above the bottom of the well in the region 96 to 111 meV.

The band discontinuity between the lowest minimum in silicon, the twofold degenerate minimum, and the lowest in $Si_{0.5}Ge_{0.5}$, the fourfold degenerate minimum, is then estimated at 105±15 meV (this shall be referred to as the conduction-band offset). This is in reasonable agreement with the value predicted by People[6] using semiclassical means of 150 meV. A summary of these estimates of the band discontinuities and a comparison with Van de Walle and Martin[7] and People[6] are shown in Table III.

TABLE III. A summary and comparison with other authors, [Van de Walle and Martin (Ref. 7) and People (Ref. 6)], of the band discontinuities estimated in the case of the 44-Å period strained calculation in the minimum-energy configuration. The explanation of how these values have been arrived at is discussed in the text.

	Our calculation	Comparison
Valence band discontinuity	353±41 meV	304 meV[a]
Conduction-band discontinuity at superlattice Γ-point minima	275±25 meV	
Conduction-band discontinuity at minima near superlattice X point	0±5 meV	
Conduction-band offset	105±15 meV	150 meV[b]

[a]Van de Walle and Martin, Ref. 7.
[b]People, Ref. 6.

E. Discussion of the optical properties

The optical matrix elements of structures comprising 52, 32, 16, and 4 atoms in the superlattice unit cell have been calculated. These are the optical transition probabilities between the uppermost valence-band superlattice state and the lowermost conduction-band state. These optical matrix elements are small because of the small degree of overlap in $\mathbf{k}$ space of the coefficients, $A_{n,\mathbf{k}}$, associated with the two states. The uppermost valence-band state is localized around Γ whereas the lowermost conduction-band state is localized near the bulk conduction minima near the X point. The optical matrix elements (presented as the normalized oscillator strengths) for the bulk $a_\perp$ strain configuration are shown in Fig. 26. There is very little difference between the two strain configurations considered here. As expected the enhancement of this optical matrix element (the zone-folding effect) is much greater in the small-period calculations.

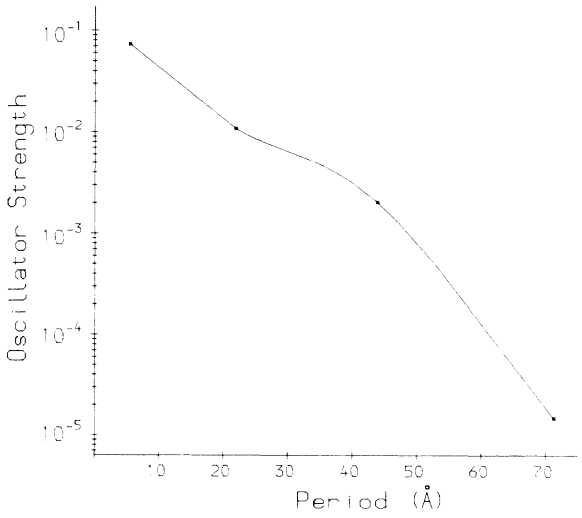

FIG. 26. A plot of the oscillator strength, associated with the transition across the fundamental superlattice gap, against the superlattice period. These are the results for the bulk $a_\perp$ strain configuration. There is very little difference between these results and the results of the minimum-energy configuration.

IV. CONCLUSIONS

In this paper we have presented band structures of $Si/Si_{0.5}Ge_{0.5}$ (001) superlattices with periods in the range 20—140 Å generated at the center of the Brillouin zone of the superlattice. A scheme involving the nearly-free-electron model was used to deal with the absolute energies of the constituents. The results presented here are in good agreement with existing experimental and phenomenological understanding of this problem. We believe that our calculation opens the way for more quantitative studies of confinement in Si-based microstructures. Our predictions can be summarized as follows:

(i) The effect of strain is to confine electrons in the silicon layers.

(ii) The separation between the confined ground state and the first excited state is increased by strain and the localization of these states in Si is enhanced. The effective height of the confining barrier at $\mathbf{k}=\mathbf{0}$ is greatly increased.

(iii) The valence- and conduction-band offsets are largely determined by volume effects and there is a simple way of evaluating them.

(iv) The evolution of the effect of confinement as a function of strain shows that strain plays an important part in determining the effective confining power of the barrier.

(v) The strain alters the fundamental superlattice gap and introduces splittings which are in good agreement with first-order (deformation-potential) theory.

(vi) The optical matrix element across the superlattice gap is enhanced by the combined effect of the microscopic superlattice potential and strain. However, its magnitude is small compared to direct-gap systems, except in structures with ultrathin (~ 10 Å) wells and barriers.

(vii) Our calculation raises the question concerning the precise relationship between the results of the rigorous local-density-functional approach and our semiempirical model for the valence-band offsets between elemental semiconductors. Although it is clear from the account given in the present study that the success of our simple model stems from the dominant role of the volume-dependent kinetic energy terms in the band structure, the degree of agreement between the two results is surprising and deserves a more thorough investigation.

ACKNOWLEDGMENT

We wish to acknowledge financial support from the Science and Engineering Research Council, United Kingdom.

[1]M. Quillec, L. Goldstein, G. Le Rout, J. Burgeat, and J. Primot, J. Appl. Phys. **55**, 2905 (1983).
[2]G. C. Osbourne, J. Appl. Phys. **53**, 1586 (1982).
[3]J. C. Bean, L. C. Feldman, A. T. Fiory, S. Nakahara, and I. K. Robinson, J. Vac. Sci. Technol. A **2**, 436 (1984).
[4]F. Cerdeira, A. Pinczuk, and J. C. Bean, Phys. Rev. B **31**, 1202 (1985).
[5]G. Abstreiter, H. Brugger, T. Wolf, H. Jorke, and H. J. Herzog, Phys. Rev. Lett. **54**, 2441 (1985).
[6]R. People, Phys. Rev. B **32**, 1405 (1985).
[7]C. G. Van de Walle and R. Martin, J. Vac. Sci. Technol. B **3**, 1256 (1985).
[8]M. Jaros, K. B. Wong, and M. A. Gell, Phys. Rev. B **31**, 1205 (1985).
[9]K. B. Wong, M. Jaros, M. A. Gell, and D. Ninno, J. Phys. C **19**, 53 (1986).
[10]I. Morrison, M. Jaros, and K. B. Wong, J. Phys. C **19**, 935 (1986).
[11]R. People and J. C. Bean, Appl. Phys. Lett. **48**, 538 (1986).
[12]V. Heine and D. Weaire, *Solid State Physics* (Academic, New York, 1970), Vol. 24, p. 53.
[13]M. Jaros, K. B. Wong, M. A. Gell, and D. J. Wolford, J. Vac. Sci. Technol. B **3**, 1051 (1985).
[14]C. G. Van de Walle and R. Martin, Phys. Rev. B **34**, 5621 (1986).